FRACTURE TOUGHNESS DISTRIBUTION IN CERAMIC-METAL FUNCTIONALLY GRADED MATERIALS

Keiichiro Tohgo*, Hiroyasu Araki*, Yoshinobu Shimamura*
*** Department of Mechanical Engineering, Shizuoka University**

Keywords: *Functionally Graded Materials, Fracture Toughness, Stable Crack Growth, Non-Graded Composites, Microstructure, Residual Stress*

Abstract

This paper deals with evaluation of fracture toughness in functionally graded materials (FGMs) consisting of partially stabilized zirconia (PSZ) and austenitic stainless steel SUS 304. FGMs and non-graded composites (non-FGMs) with fine and coarse microstructures are fabricated by powder metallurgy using PSZ and two kinds of SUS 304 powders. The fracture toughness is determined by conventional tests for several non-FGMs with each material composition and by a method utilizing stable crack growth for FGMs. Although the fracture toughness increases with an increase in a content of SUS 304 on both FGMs and non-FGMs, it is affected by microstructure and it is higher in the FGMs than in the non-FGMs. The residual stress in FGMs created in the fabrication process is estimated from the difference in fracture toughness between the FGMs and non-FGMs.

1 Introduction

Functionally graded materials (FGMs) are well known as materials in which a material composition varies gradually in some direction in order to derive the unique mechanical, thermal and electrical performances different from those of homogeneous or joined dissimilar materials. FGMs consisting of ceramics and metals, for example, can be designed to reduce thermal stress and to take advantages of the heat and corrosion resistance of ceramics and the mechanical strength of metals. Therefore, ceramic-metal FGMs are promising in thermal and structural applications such as thermal barrier coatings, wear and corrosion resistant coatings and ceramic/metal joinings [1, 2].

The ceramic-metal FGMs exhibit complicated fracture behavior due to gradation of mechanical properties and strength. In a ceramic-metal FGM plate, surface cracks emanating at the ceramic side behave in several ways depending on the material gradation and loading condition. Multiple cracks, crack arrest, crack bowing are well observed in ceramic-metal FGMs under thermal shocks or thermal fatigue [3-6]. The crack branching and spallation occurs as a result of crack growth along the interface in multi-layered FGMs [3-7]. In order to analyze the complicated fracture behavior in FGMs and to make clear fracture process and resistance of FGMs, distribution of fracture toughness in FGMs should be known.

The distribution of fracture toughness or R-curve behavior in FGMs, prediction methods based on the crack bridging model or cohesive model were proposed [8-11]. The experimental investigations on the fracture behavior of FGMs were relatively limited compared with the theoretical and numerical investigations. Several investigations have been reported using ultraviolet-irradiation-hardened polymer [12] or glass-particle reinforced epoxy [13], ceramic-metal FGMs [14-19], and ceramic-ceramic FGMs [20]. In those investigations, the distribution of fracture toughness or R-curve behavior was discussed for growing mode I crack parallel to the direction of material gradation [12, 14-17, 19,20].

In the present investigation, the distribution of fracture toughness is evaluated on two kinds of FGMs consisting of partially stabilized zirconia (PSZ) and austenitic stainless steel SUS 304. The fracture toughness is determined by conventional tests for several non-graded composites (non-FGMs) with each material composition and by a method utilizing stable crack growth for FGMs. Based on the experimental results, fracture mechanism and influences of microstructure on fracture toughness distribution in FGMs have been discussed. Finally, the residual stress in FGMs created in the fabrication process is estimated from the difference in fracture toughness between the FGMs and non-FGMs.

2 Materials and Experimental Procedure

2.1 Materials

The tested materials were FGMs and non-graded composites (non-FGMs) fabricated by powder metallurgy. Row materials were commercially available partially stabilized zirconia (ZrO_2-3molY_2O_3, PSZ) and austenitic stainless steel (SUS 304) powders. The mean particle sizes of powders were 0.32μm for the PSZ and 45μm and 10μm for the SUS 304, respectively. The PSZ and SUS 304 powders were mixed in volume ratios of 10-0, 8-2, 6-4, 4-6, 2-8, 1-9 and 0-10, respectively, and each mixture was suspended in isopropyl alcohol, milled for three hours by a vibrational ball mill and dried. The powder blends were put to form a non-graded composition or were layered to form a graded composition in a graphite die with 30mm in diameter. The powder compacts were pressed up to 14MPa at room temperature, and then sintered under the condition of 1200ºC and 30MPa for one hour by a hot-press machine. Finally, seven kinds of non-FGMs and FGM were obtained for each combination of powders. These materials are referred to as non-FGM(45μm), FGM(45μm), non-FGM(10μm) and FGM(10μm), respectively. Fig. 1 shows microstructures of the non-FGM(45μm) and non-FGM(10μm). The white and gray regions exhibit the SUS 304 and PSZ phases, respectively. The non-FGM(10μm) and non-FGM(45μm) have fine and coarse microstructures, respectively. SUS 304 particles are dispersed in the PSZ matrix in the material with high content of PSZ (80%PSZ), while small PSZ particles and platelets are dispersed in the SUS 304 matrix in the material with low content of PSZ (20%PSZ). Area fractions of PSZ and SUS 304 phases in the microstructures were measured by image processing, and used as effective volume fractions. The FGMs have a functionally graded layer (FGM layer) of nominally 2mm in thickness on a SUS 304 substrate. Fig. 2 shows the area fraction of SUS 304 as a function of a distance from ceramic surface in both FGMs. The gradation of material composition is more or less steeper in the FGM (45μm) than in the FGM (10μm).

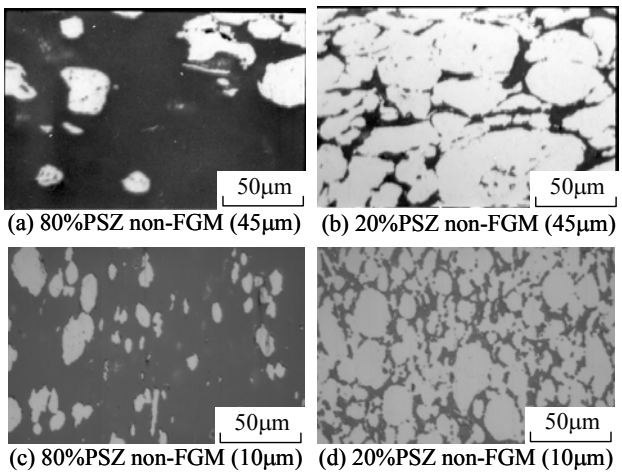

(a) 80%PSZ non-FGM (45μm) (b) 20%PSZ non-FGM (45μm)
(c) 80%PSZ non-FGM (10μm) (d) 20%PSZ non-FGM (10μm)

Fig. 1. Microstructures of the materials.

2.2 Experimental procedure

Rectangular specimens were cut out from the disks and polished with diamond powder paste (particle size: 5μm). Fracture toughness tests of the non-graded materials were carried out on three-point-bending specimens with a sharp edge notch as in Fig. 3(a) [21]. To evaluate the fracture toughness distribution in the FGMs, stable crack growth tests were conducted on three-point-bending specimen with a series of median cracks by Vickers indentation on the ceramic surface [19]. These tests were conducted at a cross head speed of 0.05mm/min and room temperature. During the tests, the relationship between load (P) and load-point displacement (δ) was recorded, and the image of crack initiation and growth on the side-surface of the specimens was monitored and recorded in video recorder through a CCD camera. The test and video recording were started at the same time and the time was measured through the test so that the fracture process could be investigated in detail after the test.

3 Fracture Toughness of Non-FGM

The load vs. load-point displacement relations obtained by the fracture toughness tests of the non-FGM(45μm) are shown in Fig. 4 [21]. In this figure, fracture process around a notch tip in the 10%PSZ is

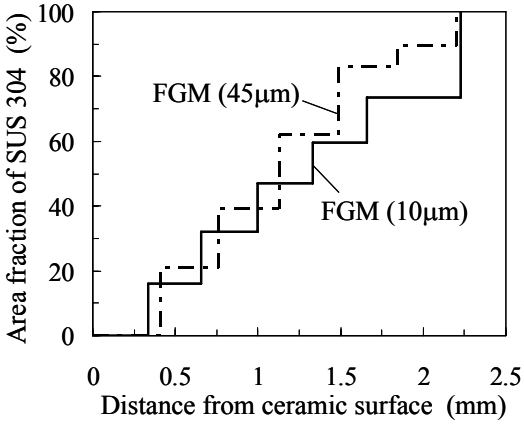

Fig. 2. Area fractions of SUS 304 as functions of distance from ceramic surface in FGMs

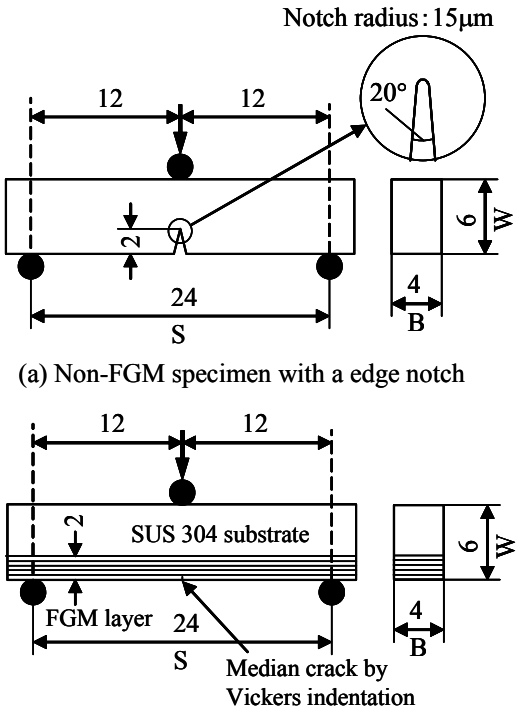

Fig. 3 Specimen configurations. (dimensions in mm)

schematically illustrated based on the observation by a CCD camera. Fracture process accompanied with the load-displacement relation on the 10%PSZ is described as follows. The applied load increased linearly against the displacement up to a point A in Fig. 4, and then the load-displacement relation became nonlinear and a dent of the side surface corresponding to the plastic deformation around a notch-tip was observed. In the composites with low PSZ content, as the matrix material was SUS 304, the plastic deformation occurred in the matrix around a notch-tip at this stage. At a point B before the maximum load (point C) a crack was initiated from a notch tip, and the load decreased with crack growth after the point C. Although the knee point corresponding to plastic deformation was not observed on the load-displacement relations of the non-FGMs with higher PSZ content than 40%, the crack initiation and extension before the maximum load were observed in all specimens except for the monolithic PSZ specimen. The monolithic PSZ exhibited unstable fracture at the maximum load.

Two kinds of critical stress intensity factors (K_{R0} and K_R) were obtained from the load for crack initiation and initial notch length and from the maximum load and current crack length, respectively. As the sharp edge notch was regarded as a crack, K_{R0} corresponds to the fracture toughness

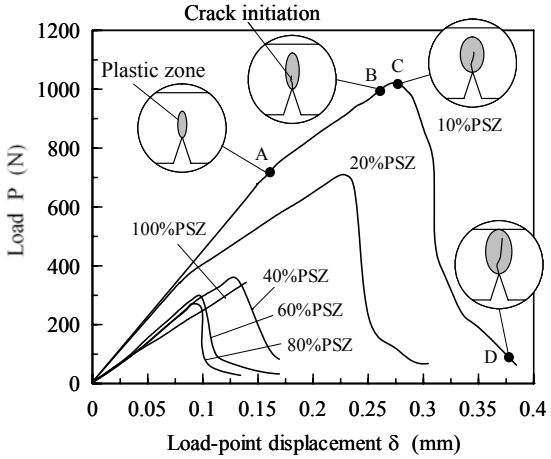

Fig. 4. Load vs. load-point displacement relations in fracture toughness tests of non-graded composites.

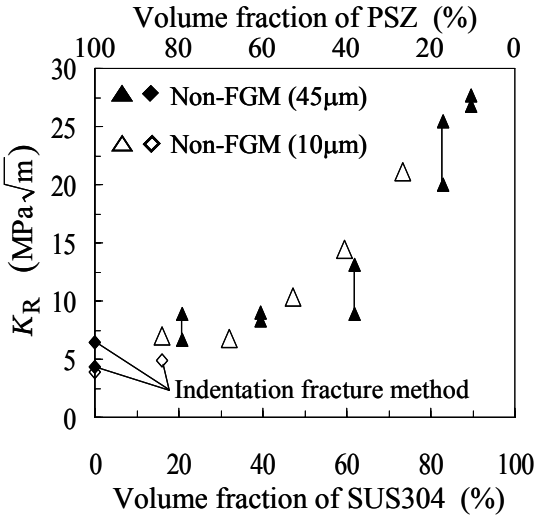

Fig. 5. Fracture toughness as a function of material composition in non-FGMs.

for crack initiation while K_R corresponds to the fracture toughness for crack extension. The K_R values are plotted against the material composition of the non-FGM(45μm) and non-FGM(10μm) in Fig. 5. For the monolithic PSZ and non-FGM(10μm) with 80%PSZ, the fracture toughness obtained by the indentation fracture method is plotted, because the sharp notch with notch radius of 15μm still can not be regarded as a crack for these materials. The fracture toughness increases with an increase in metal phase content in both non-FGM(45μm) and non-FGM(10μm), and a little difference between both non-FGMs suggests a little influence of microstructure on the fracture toughness.

4 Fracture Toughness of FGM

4.1 Stress intensity factor of a crack in FGM

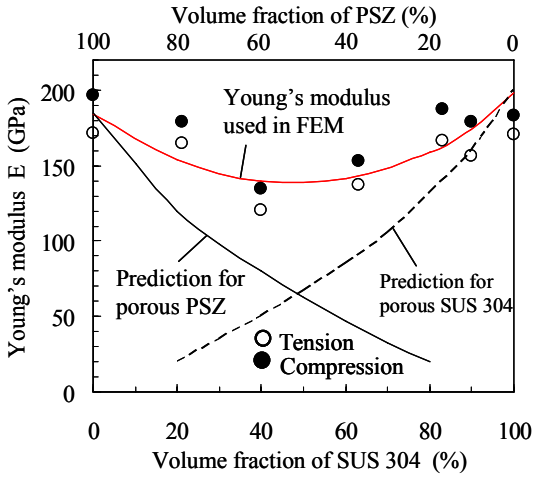

Fig. 6. Young's modulus as a function of material composition.

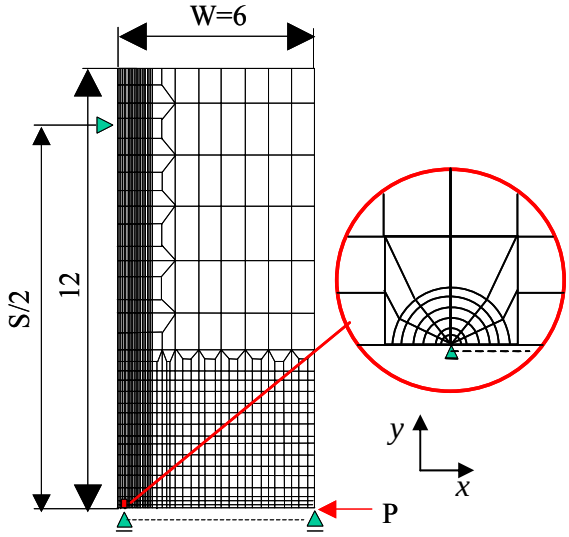

Fig. 7. Finite element mesh of three-point bending specimen.

Since the elastic moduli are graded corresponding to gradation of material composition in FGMs, the stress intensity factor of a crack in FGMs should be analyzed for each FGM even if their specimen configuration and loading condition are the same. In the present material system, the gradation of Young's modulus may not be significant because of the slight difference in the Young's modulus between PSZ and SUS 304, namely 190 GPa for PSZ and 200 GPa for SUS 304 [19, 21]. Therefore, the stress intensity factor for homogeneous materials can be approximately used as in reference [19]. However, according to the experimental results of four-point-bending tests of non-FGMs, the Young's modulus exhibits low value in the composites with intermediate composition as

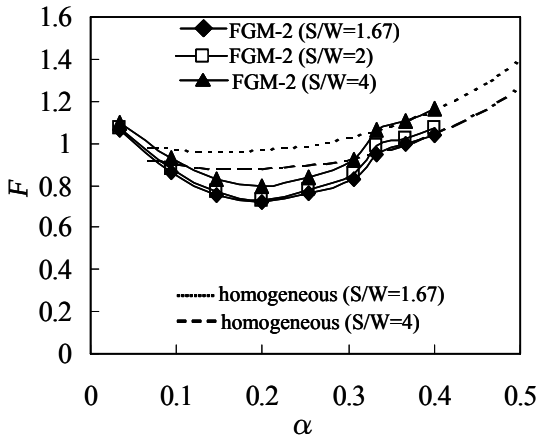

Fig. 8. Correction factors of stress intensity in three-point bending FGM specimens.

shown in Fig. 6. This suggests that the initial defects are contained in the composites or the interfacial strength between both phases is very low.

Therefore, the stress intensity factor of a crack in three-point-bending FGM specimens were analyzed with a finite element method taking into account the variation of Young's modulus corresponding to material composition in FGMs. Fig. 7 shows the finite element mesh of three-point-bending specimen, where the Young's modulus is assigned to the Gauss points of each mesh based on the material composition and Fig. 6. The stress intensity factor K is determined by extrapolation of K' $\left(=\sigma_y\sqrt{2\pi r}\right)$ to a crack tip, where σ_y is the normal stress in y direction at the position of x ahead of a crack tip. The correction factor is defined by

$$F = \frac{K}{\sigma_0\sqrt{\pi a}}\ , \qquad (1)$$

$$\sigma_0 = \frac{3PS}{2W^2B}\ , \qquad (2)$$

where P, a, S, W and B are the applied load, crack length, span length, width and thickness of the three-point bending edge crack specimen, respectively.

Fig. 8 shows the correction factors as functions of normalized crack length $\alpha(=a/W)$ for a crack in the three-point bending FGM specimens. In the figure the correction factors for the homogeneous materials are also shown. As sown in Fig. 8, the correction factors for the FGM specimens decrease in the FGM layer, and they are consistent with those for homogeneous materials when the crack length is beyond the FGM layer

4.2 Fracture toughness of FGM

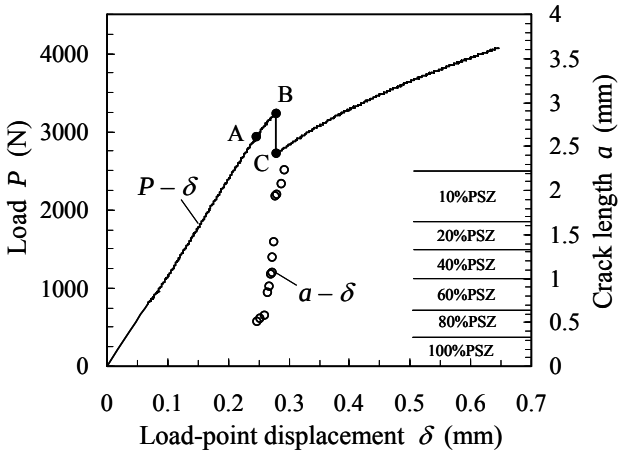

Fig. 9. Load and crack length vs. load- point displacement in FGM(10μm).

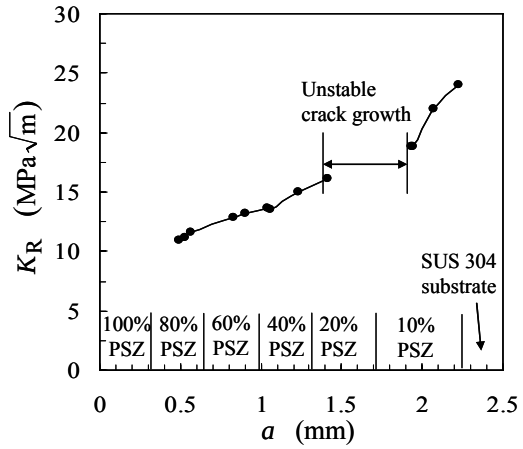

Fig. 10. Distribution of fracture toughness in FGM(10μm).

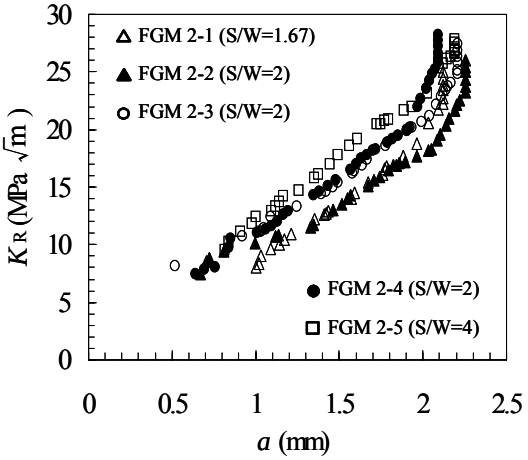

Fig. 11. Distributions of fracture toughness in FGM(45μm).

On the three-point-bending test of a FGM specimen with a short crack in the ceramic side surface as in Fig. 3(b), stable crack growth in a FGM layer is realized depending on the distribution of material composition, specimen size, etc. Since the stress intensity factor during stable crack growth exhibits the fracture resistance at the crack-tip region, the distribution of fracture toughness in the FGM layer is obtained [19].

Fig. 9 shows the load and crack length vs. load-point displacement relation obtained by three-point-bending test of the FGM(10μm). When the applied load reached a point A in Fig. 9, the stable crack growth started from a pre-crack. After the crack stably extended to 1.4mm in crack length at a point B, unstable crack growth occurred to 1.9mm in crack length and the load dropped down to a point C. Then, the crack stably extended again to the interface between the FGM layer and the SUS 304 substrate, and the large plastic deformation spread into the substrate. In the FGM(10μm) specimen, the stable crack growth was hard to occur and was realized in only one specimen shown in Fig. 9 out of several specimens. On the other hand, all FGM(45μm) specimens exhibited the stable crack growth as reported in the reference [19].

From the relationship between applied load and crack length during the stable crack growth, the critical stress intensity factor (K_R) was calculated. The correction factor in Fig. 8 for the three-point-bending FGM specimens was used to calculate K_R. Fig. 10 shows the fracture toughness K_R as a function of the crack length, i.e. the distance from the ceramic surface for the FGM(10μm) specimen in Fig. 9. The fracture toughness between 1.4mm and 1.9mm in crack length is not obtained because of unstable crack growth. Fig. 11 shows the fracture toughness as a function of the crack length for the FGM(45mm) specimens [19]. The gradient of the

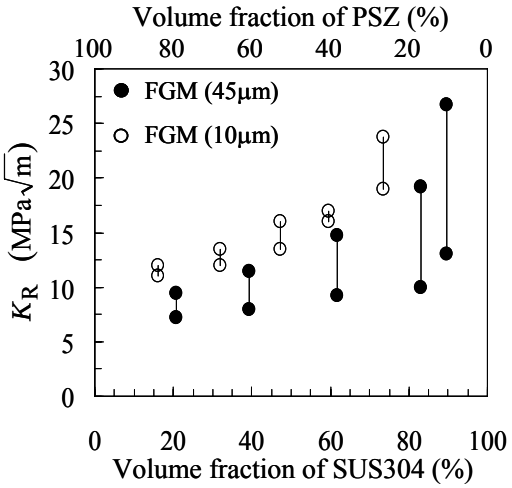

Fig. 12. Fracture toughness as a function of material composition in FGMs.

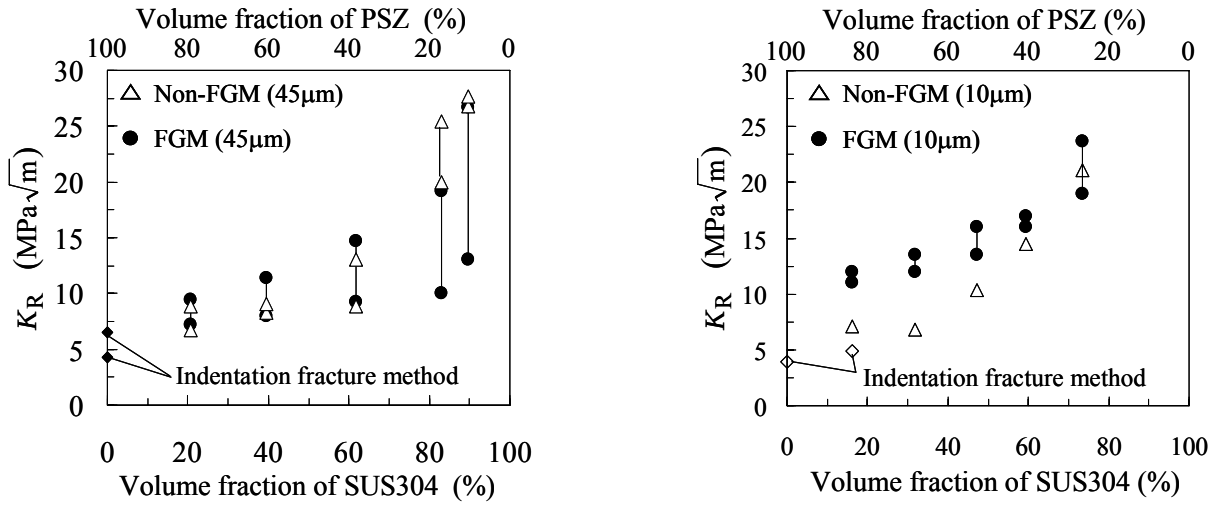

(a) Non-FGM (45μm) and FGM(45μm) (b) Non-FGM (10μm) and FGM(10μm)

Fig. 13. Comparison of fracture toughness between non-FGM and FGM.

fracture toughness in the FGM layer for the FGM(10μm) is not severe as compared to that for the FGM(45μm), and therefore the stable crack growth was hard to be realized in the FGM(10μm). From these data, the relationship between the fracture toughness and material composition is obtained as in Fig. 12 for both FGM(10μm) and FGM(45μm). Although the fracture toughness increases with an increase in the SUS 304 volume fraction in both FGMs, it is higher in the FGM(10μm) than in the FGM(45μm) in contrast with the case of the non-FGMs.

4.3 Comparison of the fracture toughness between the non-FGMs and FGMs

Figs. 13(a) and (b) show the comparison of the fracture toughness between the non-FGM and FGM for the cases of 45μm and 10μm in particle size of SUS 304 powder, respectively. In the case of 45μm in Fig.12(a), data points of the non-FGM are within the data band of the FGM. On the other hand, in the case of 10μm in Fig. 13(b), the fracture toughness of the FGM is much higher than that of the non-FGM.

5 Estimation of Residual Stress in FGMs

In general FGMs, the compressive residual stress is created in the ceramic rich region due to mismatch of the thermal expansion coefficients of ceramic and metal phases in the fabrication. Since the fracture toughness of the FGMs contains the effect of the residual stress, it is higher than that of the non-FGMs. Here, the residual stress in the FGMs is estimated from the difference in fracture toughness between the FGMs and non-FGMs. Fig. 14 shows a schematic illustration of fracture toughness distribution in FGMs. $K_R^{FGM}(x)$ is an actual distribution and $K_R^{Non\text{-}FGM}(x)$ is obtained based on the fracture toughness of non-FGM and graded material composition. In the estimation a smoothing curve of stepwise $K_R^{Non\text{-}FGM}(x)$ is used. The difference in fracture toughness distributions is given as:

$$K_{Res}(x) = K_R^{Non-FGM}(x) - K_R^{FGM}(x) \qquad (3)$$

It is assumed that $K_{Res}(x)$ is due to the residual stress $\sigma_{Res}(x)$. The stress intensity factor of a crack under residual stress distribution is obtained by the one of a crack subjected to the same stress distribution on crack surfaces from the principle of superposition as shown in Fig. 15. In order to estimate the stress intensity factor of a crack in Fig. 15 (c), the result for an edge crack in semi-finite plate subjected to

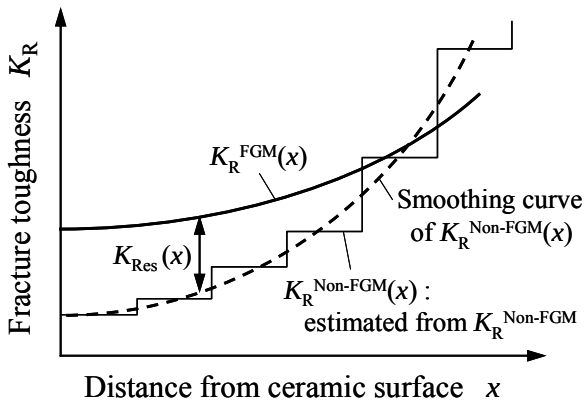

Fig. 14. Schematic illustration of fracture toughness distribution in FGMs. $K_R^{FGM}(x)$ is an actual distribution and $K_R^{Non\text{-}FGM}(x)$ is obtained based on the fracture toughness of non-FGM and graded material composition.

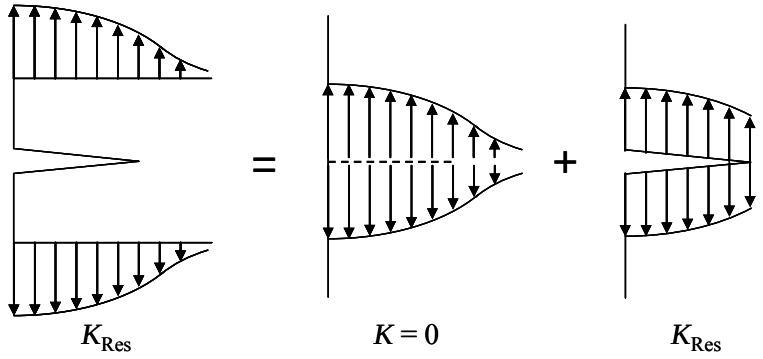

Fig. 15. Principle of superposition for a crack under residual stress distribution.

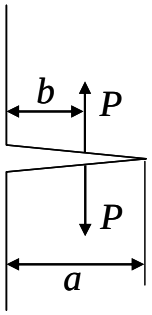

Fig. 16. An edge crack in semi-finite plate subjected to concentrated forces on the crack surfaces

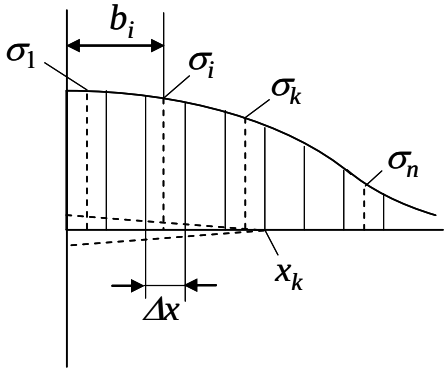

Fig. 17 A crack under residual stress distribution.

concentrated forces on the crack surfaces as in Fig. 16 is used [22]. The stress intensity factor is given as

$$K_I = \frac{2P}{\sqrt{\pi a}} \frac{F(b/a)}{\sqrt{1-(b/a)^2}} \tag{4}$$

$$F(\alpha) = 1 + (1-a^2)\,(0.2945 - 0.3912\alpha^2 + 0.7685\alpha^4 - 0.9942\alpha^6 + 0.5094\alpha^8) \tag{5}$$

$$\alpha = b/a \tag{6}$$

The residual stress distribution, namely the stress distribution on the crack surfaces in Fig. 15 is discretized as shown in Fig. 17. When the crack length is x_k, the stress intensity factor of a crack subjected to the stress distribution on the crack surfaces is obtained as

$$K_{Res}(x_k) = \sum_{i=1}^{k} \frac{2\,\sigma_i\,\Delta x\,F(b_i/x_k)}{\sqrt{\pi x_k}\sqrt{1-(b_i/x_k)^2}} \tag{7}$$

From the above equation, the residual stress σ_k at the position b_k is described by the following relation.

$$\sigma_k = \frac{\sqrt{\pi x_k}\sqrt{1-(b_k/x_k)^2}}{2\,\Delta x\,F(b_k/x_k)} \times \left\{ K_{Res}(x_k) - \sum_{i=1}^{k-1} \frac{2\,\sigma_i\,\Delta x\,F(b_i/x_k)}{\sqrt{\pi x_k}\sqrt{1-(b_i/x_k)^2}} \right\} \tag{8}$$

As $K_{Res}(x_k)$ is known, the residual stress σ_1 at b_1 is given as

$$\sigma_1 = \frac{\sqrt{\pi x_1}\sqrt{1-(b_1/x_1)^2}}{2\,\Delta x\,F(b_1/x_1)} K_{Res}(x_1) \tag{9}$$

Then, as σ_1 is obtained by Eq. (9), the σ_2 at b_2 is given by

$$\sigma_2 = \frac{\sqrt{\pi x_2}\sqrt{1-(b_2/x_2)^2}}{2\,\Delta x\,F(b_2/x_2)} \times \left\{ K_{Res}(x_2) - \frac{2\,\sigma_1\,\Delta x\,F(b_1/x_2)}{\sqrt{\pi x_2}\sqrt{1-(b_1/x_2)^2}} \right\} \tag{10}$$

By continuing this procedure up to i=n, the residual stress distribution is obtained.

In the numerical calculation, the distributions of K_{Res} in Fig. 18 is used for the FGM(10μm) and FGM(45μm), and n=200 is set for the FGM layer of 2mm. The obtained results are shown in Fig. 19. The reasonable results are obtained: the residual stress in the FGMs is compression at the ceramic-rich surface region, and decreases and turns to tension with going through the inside. The compressive residual stress at the surface region is much higher in the FGM(10μm) than in the FGM(45μm). This might be attributed to the size effect of microstructure and the gradation of material composition in both FGMs.

6 Conclusions

In order to evaluate the distributions of fracture toughness in the PSZ-SUS 304 FGMs, fracture toughness tests were carried out on the non-FGMs

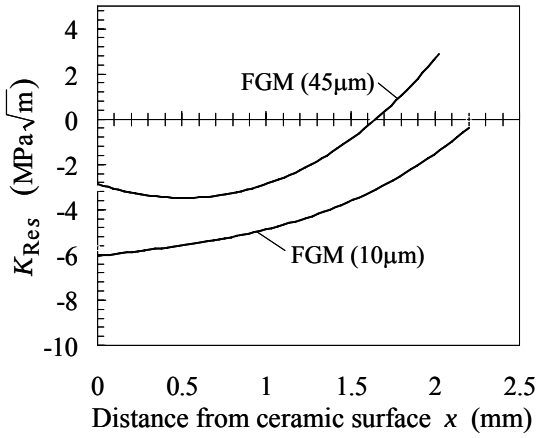

Fig. 18. Difference of fracture toughness between FGM and Non-FGM.

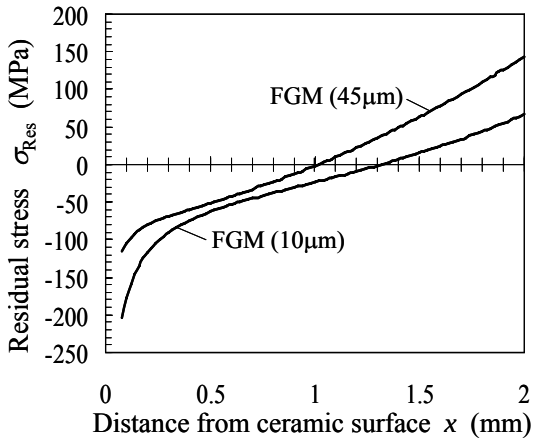

Fig. 19. Distributions of residual stress in FGMs.

and FGMs. The obtained results are summarized as follows:

(1) The fracture toughness obtained by the non-FGMs and FGMs increases with an increase in a SUS 304 volume fraction.

(2) On the fracture toughness of the non-FGMs, the influence of microstructure is negligible.

(3) On the FGMs, the fracture toughness is higher in the FGM with fine microstructure than in the FGM with coarse microstructure.

(4) The fracture toughness in the FGMs is higher than that of the non-FGM especially in the case of fine microstructure, and this may be attributed to the compressive residual stress in the ceramic rich region in the FGMs.

(5) The residual stress in the FGMs is estimated from the difference in fracture toughness between the FGMs and non-FGMs. As a results, the compressive residual stress at the surface region is much higher in the FGM with fine microstructure than in the FGM with coarse microstructure.

References

[1] Takahashi H, Hashida T. "Development of an evaluation method of functionally gradient materials". *JSME Int. J., Ser. A*, Vol.33, pp 281-287, 1990.

[2] Miyamoto Y., Kaysser W.A., Rabin B.H., Kawasaki A., and Ford R.G. *"Functionally Graded Materials: Design, Processing and Applications"*, Kluwer Academic Publishers, 1999.

[3] Kawasaki A., Watanabe R., Yuuki M., Nakanishi Y. and Onabe H. "Effects of microstructure on thermal shock cracking of functionally graded thermal barrier coatings studied by burner heating test. Materials". *Trans. JIM*, Vol.37, pp 788-795, 1996.

[4] Kawasaki A. and Watanabe R. "Thermal fracture behavior of metal/ceramic functionally graded materials". *Eng. Frac. Mech.*, Vol.69, pp 1713-1728, 2002.

[5] Rangaraj S. and Kokini K. "Estimating the fracture resistance of functionally graded thermal barrier coatings from thermal shock tests". *Surf. Coat. Technol.*, Vol. 173, pp 201-212, 2003.

[6] Bahr H.A., Balke H., Fett T., Hofinger I., Kirchhoff G., Munz D., Neubrand A., Semenov A.S., Weiss H.J. and Yang Y.Y. "Cracks in functionally graded materials". *Mater. Sci. Eng.*, Vol. A362, pp 2-16, 2003.

[7] Tohgo K. and Hadano A. "Characterization of Fracture Process in Ceramic-Metal Functionally Graded Material under Three-Point-Bending". *JSME Int. J., Ser. A*, Vol.49, pp 321-330, 2006.

[8] Jin Z.H. and Batra R.C. "Some basic fracture mechanics concepts in functionally graded materials". *J. Mech. Phys. Solids*, Vol. 44, pp 1221-1235, 1996.

[9] Jin Z.H., Paulino G.H. and Dodds Jr. R.H. "Cohesive fracture modeling of elastic-plastic crack growth in functionally graded materials". *Eng. Frac. Mech.*, Vol. 70, pp 1885-1912, 2003.

[10] Jin Z.H. and Batra R.C. "R-curve and strength behavior of a functionally graded material". *Mater. Sci. Eng.*, Vol. A242, pp 70-76, 1998.

[11] Cai H. and Bao G. "Crack bridging in functionally graded coatings". *Int. J. Solids Struct.*, Vol. 35, pp 701-717, 1998.

[12] Li H., Lambros J., Cheeseman B.A. and Santare M.H. "Experimental investigation of the quasi-static fracture of functionally graded materials". *Int. J. Solids Struct.*, Vol. 37, pp 3715-3732 , 2000.

[13] Rousseau C.E. and Tippur H.V. "Compositionally graded materials with cracks normal to the elastic gradient". *Acta Mater.*, Vol. 48, pp 4021-4033, 2000.

[14] Tomsia A.P., Saiz E., Ishibashi H., Diaz M., Requena J. and Moya J.S. "Powder Processing of Mullite/Mo functionally graded materials". *J. Eur. Ceram. Soc.*, Vol. 18, pp 1365-1371, 1998.

[15] Rodriguez-Castro R., Wetherhold R.C. and Kelestemur M.H. "Microstructure and mechanical behavior of functionally graded Al A359/SiC_p composite". *Mater. Sci. Eng.*, Vol. A323, pp 445-456, 2002.

[16] Lin J.S. and Miyamoto Y. "Notch effect of surface compression and the toughening of graded Al_2O_3/TiC/Ni materials". *Acta Mater.*, Vol. 48, pp 767-775, 2000.

[17] Lin C.Y., McShane H.B. and Rawlings R.D. "Structure and properties of functionally gradient aluminium alloy 2124/SiC composites". *Mater. Sci. Technol.*, Vol. 10, pp 659-664, 1994.

[18] Fukui Y. and Bowen P. "Fatigue crack propagation in an in-situ Al-Al_3Ni functionally gradient material". *Trans. Jpn. Soc. Mech. Eng., Ser. A*, Vol. 60, pp 2048-2053, 1994.

[19] Tohgo K., Suzuki T. and Araki H. "Evaluation of R-curve behavior of ceramic-metal functionally graded materials by stable crack growth", *Eng. Frac. Mech.*, Vol. 72, pp 2359-2372, 2005.

[20] Moon R.J., Hoffman M., Hilden J., Bowman K.J., Trumble K.P. and Rodel J. "R-curve behavior in alumina-zirconia composites with repeating graded layers". *Eng. Frac. Mech.*, Vol. 69, pp 1647-1665, 2002.

[21] Tohgo K. and Kawaguchi T. "Influence of material composition on mechanical properties and fracture behavior of ceramic-metal composites", *Key Engineering Materials*, Vols. 297-300, pp 1516-1521, 2005.

[22] Hartranft R.J. and Sih G.C.*"Method of Analysis and Solutions of Crack Problems"*. Sih G.C. ed. Noordhoff, Holland, 1973.